Pseudogap in the density of states and the highest Néel temperature of the $L1_0$-type MnIr alloy system

R. Y. Umetsu, M. Miyakawa, and K. Fukamichi
Department of Materials Science, Graduate School of Engineering, Tohoku University, Aoba-yama 02, Sendai, 980-8579, Japan

A. Sakuma
Department of Applied Physics, Graduate School of Engineering, Tohoku University, Aoba-yama 08, Sendai 980-8579, Japan
(Received 12 July 2003; revised manuscript received 2 October 2003; published 17 March 2004)

The Néel temperature T_N, electronic specific heat coefficient γ_e, band structures and the effective exchange constant J_0 of the $L1_0$-type MnIr alloy system have been investigated. The value of T_N is highest among Mn alloy systems, being 1145 K for the alloy with 50.1% Ir. The temperature dependence of electrical resistivity exhibits a hump just below T_N and the experimental electronic specific heat coefficient γ_e is small of $2-3\ \mathrm{mJ\,mol^{-1}\,K^{-2}}$, characteristic to pseudo-gap-type antiferromagnets, though γ_e is rather larger than that of other $L1_0$-type Mn alloy systems. In addition, the concentration dependences of T_N and γ_e are not so sensitive to the Ir concentration. These behaviors are well explained by the theoretical calculations, that is, a pseudogap is formed around the Fermi level E_F and the total density of states of the equiatomic MnIr alloy in the antiferromagnetic state is about 6 states $\mathrm{Ry^{-1}\,atom^{-1}\,spin^{-1}}$, corresponding to about $1\ \mathrm{mJ\,mol^{-1}\,K^{-2}}$ of the calculated electronic specific heat coefficient γ_e^{cal}. The Néel temperature T_N^{cal} calculated from J_0 in the molecular field approximation is 1495 K, highest among several kinds of the $L1_0$-type equiatomic Mn alloy systems. From the calculated results of T_N^{cal} under the different additive element and/or the lattice constants, it is concluded that the magnitude of the Néel temperature T_N of the $L1_0$-type equiatomic Mn alloy systems is explained by the J_0 curve which reflects the difference in the number of electrons at the Mn site.

DOI: 10.1103/PhysRevB.69.104411 PACS number(s): 75.50.Ee; 75.40.−s

I. INTRODUCTION

Several kinds of equiatomic Mn alloys with Ni, Pd, Pt, Rh, and Ir have the $B2$ (CsCl)-type cubic phase at high temperatures and transform to the $L1_0$ (CuAu-I)-type tetragonal phase with a diffusionless martensitic transformation process at low temperatures.[1–4] From neutron diffractions and magnetic data, it has been reported that the $L1_0$-type phase exhibits a collinear antiferromagnetic structure and the equiatomic MnNi,[5] MnPd,[5,6] and MnPt (Refs. 5, 7, 8) alloys have a very high Néel temperature T_N of about 1070, 810, and 970 K, respectively. Recent theoretical investigations have demonstrated that the density of states (DOS) of the $L1_0$-type equiatomic MnNi,[9] MnPd,[10] and MnPt (Ref. 11) alloys exhibit a pseudogap around the Fermi level E_F. The formation of the pseudogap is attributed to the antiferromagnetic staggered field due to the antiferromagnetic spin arrangements, and hence no pseudogap is formed in the paramagnetic states as well as the ferromagnetic state. In fact, the experimental data for these equiatomic alloys show the characteristic behaviors of the pseudogap-type antiferromagnets such as a substantially small electronic specific heat coefficient γ_e (Refs. 10, 12) and a clear hump just below T_N in the electrical resistivity (ρ)–temperature (T) curves.[10,12] Such characteristic band structure is common to the $L1_0$-type equiatomic MnNi, MnPt, and MnPd alloys with the same crystal structure.[9–12] Accordingly, it is considered that the high stability of antiferromagnetism for these alloys is closely correlated to the band structure.

Recently, due to a high stability of antiferromagnetism, especially, MnPt alloy system has been intensively investigated from the viewpoint of practical applications such as a pinning layer of giant magnetoresistance (GMR) (Refs. 13–16) and tunnel magnetoresistance (TMR) devices.[17–19] The γ-phase of the Mn–Ir alloy system is also attractive for the pinning layer, because excellent properties are obtained without postannealing.[20–24] On the other hand, the equiatomic MnIr alloy system has scarcely been investigated for the electric devices mentioned above, although the $L1_0$-type MnIr alloy is known to be antiferromagnetic at room temperature from neutron diffractions.[25] Since the magnetic data in 1960s suggest that T_N is above 1100 K,[26] the $L1_0$-type MnIr alloys in the vicinity of the equiatomic composition would be expected to have a very high antiferromagnetic stability.

In the present study, we have investigated the electrical resistivity and the low temperature specific heat capacity of the $L1_0$-type MnIr alloy system in order to investigate the Néel temperature T_N and the electronic state. Furthermore, the band structures and the effective exchange constant J_0 which gives an estimation of T_N are calculated by the tight-binding linear muffin-tin orbital (LMTO) method with the local spin density (LSD) functional approximation.[9,11,27,28]

II. EXPERIMENT AND THEORETICAL CALCULATION METHOD

A. Experimental procedure

Several kinds of the specimens were prepared by arc-melting in an argon gas atmosphere and annealed at 1073 K for 72 h in vacuum sealed quartz tubes and slowly cooled down to room temperature. Their crystal structure was identified as an $L1_0$-type single phase and the room temperature lattice constant was obtained by x-ray powder diffraction.

The mass density of the specimens was examined by using toluene as a working liquid. The alloy compositions were confirmed by an inductively coupled plasma (ICP) analysis and also decided from the density derived from the lattice constants. The electrical resistivity from room temperature up to 1300 K was measured by a conventional four-probe method. In the x-ray diffractions at high temperatures, a tantalum sheet and its diffractions were used as a sample stage and a reference, respectively. The low-temperature specific heat capacity measurements from 2 to 10 K were carried out by a thermal relaxation method.

B. Outline of theoretical calculation method

For the electronic structure calculations, the linear muffin-tin orbital (LMTO) method is employed within the framework of the local spin density (LSD) functional formalism. After accomplishing the self-consistent calculations, we further evaluate the Néel temperature in order to examine the stability of the magnetic structure by using the effective exchange constant given by the following equation:[27,28]

$$J_i = -\frac{1}{4\pi}\mathrm{Im}\int^{E_F} d\omega \mathrm{Tr}_{\mathrm{Im}}\{\Omega_i(\omega)[g_{ii}^{\gamma\uparrow\uparrow}(\omega) - g_{ii}^{\gamma\downarrow\downarrow}(\omega)] + \Omega_i(\omega) g_{ii}^{\gamma\uparrow\uparrow}(\omega)\Omega_i(\omega) g_{ii}^{\gamma\downarrow\downarrow}(\omega)\}. \quad (1)$$

The quantity J_i can be regarded as the amplitude of the exchange field acting on an atom denoted by i by surrounding moments. In the above equation,

$$\Omega_i(\omega) \equiv [p_i^{\gamma\uparrow}(\omega) - p_i^{\gamma\downarrow}(\omega)], \quad (2)$$

where $p^{\gamma}(\omega)$ is the potential function given by $p^{\gamma}(\omega) = \{(\omega - C)/\Delta\}\delta_{L',L}\delta_{\sigma',\sigma}$, and $g_{ii}^{\gamma\sigma\sigma'}(\omega) = [(p^{\gamma}(\omega) - S^{\gamma})^{-1}]_{ii}^{\sigma\sigma'}$ is the so-called auxiliary Green function, in the tight-binding LMTO scheme, constituted of the potential function $p^{\gamma}(\omega)$ and S^{γ} the screened structure constants given by $S^{\gamma} = S(1-\gamma S)^{-1}$. Here, we define $L = (i,l,m)$ (i denotes the site, l and m are orbital indices) and σ as the spin state, the quantities C, Δ, and γ are the potential parameters determined within each atomic sphere by using the LSD. Using J_i, the Néel temperature T_N is obtained by the following expression based on the generalized molecular field theory by Liechtenstein *et al.*:[27]

$$T_N = \frac{2J_0}{3k_B}. \quad (3)$$

The tight-binding LMTO method is also useful for the treatment of the substitutional disordered system in which we can apply the coherent potential approximation (CPA).[29] In the present work, we perform the CPA calculations in the paramagnetic state, regarded as a disordered local moment (DLM) state where the moment directions are randomly distributed.

III. RESULTS AND DISCUSSION

Figures 1(a) and 1(b) show the temperature T dependence of electrical resistivity ρ of the $L1_0$-type MnIr alloys with less (a) and more (b) than half of the Ir concentration, respectively. The $\rho - T$ curves exhibit a hump, and additionally show a hysteresis at higher temperatures for 40.2% and 41.6% Ir. These behaviors are similar to those of the pseudogap-type antiferromagnetic MnPd alloy system in which the phase transformation from the $B2$-type to the $L1_0$-type structure takes place above T_N.[10] The concentration dependence of the mass density and the room temperature lattice constants are in good agreement with the previous data in the literature.[26] In Fig. 2, we set representative x-ray powder diffraction patterns of the $L1_0$-type MnIr alloy with 40.2% Ir. The upper and lower patterns are the results at room temperature (R.T.) and at 1273 K, respectively. The former can be identified as a single phase of the $L1_0$-type structure and the latter is as a mixed phase of the $L1_0$-type structure with the $B2$-type structure. Although the diffraction patterns at higher temperatures above 1273 K cannot be obtained because of our experimental limitation, it is clear that the hysteresis in the $\rho - T$ curves corresponds to the phase transition, and the transition temperature is in accordance with that in the phase diagram of the Mn–Ir alloy system.[4] In other MnIr alloys in Figs. 1(a) and 1(b), no x-ray powder

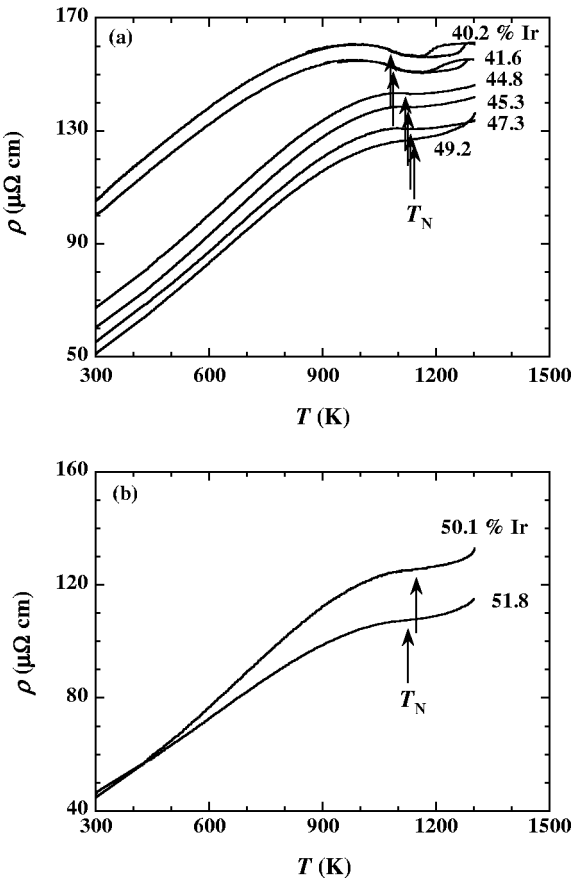

FIG. 1. Temperature dependence of electrical resistivity ρ of several kinds of the $L1_0$-type MnIr alloys with less (a) and more (b) than half of the Ir concentration, respectively. The arrows indicate the Néel temperature T_N defined from the minimum point in the temperature derivative of the electrical resistivity–temperature curves.

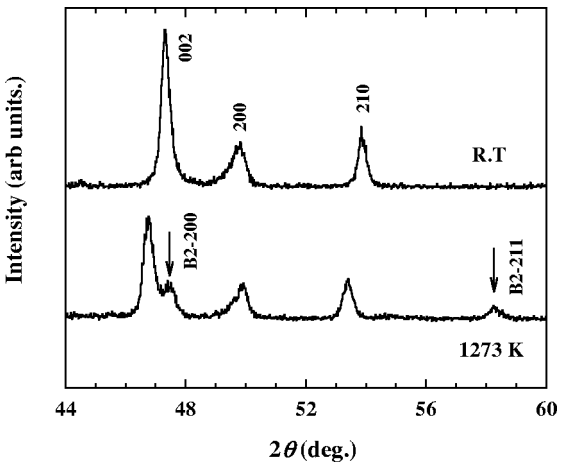

FIG. 2. X-ray powder diffraction patterns of the $L1_0$-type MnIr alloy with 40.2% Ir. The upper and lower patterns were measured at room temperature (R.T.) and 1273 K, respectively.

diffraction patterns corresponding to the $B2$-type structure have been confirmed up to around 1250 K. From room temperature neutron diffraction data, it has been reported that the $L1_0$-type MnIr alloy has a collinear antiferromagnetic spin structure.[25] Therefore, it is regarded that the hump in the $\rho-T$ curves is associated with the appearance of T_N. In general, the feature of ρ at T_N in antiferromagnets depends on the periodicity and dimensionality of their magnetic structure. Using the following scaling of the critical exponents, α_c, β_c, and γ_c with $\alpha_c+2\beta_c+\gamma_c=2$, the temperature derivative of resistivity $d\rho/dT$ is expressed as[30,31]

$$d\rho/dT=-A\varepsilon^{-(\alpha_c+\gamma_c)/2}+B\varepsilon^{-(\alpha_c+\gamma_c-1)}(T<T_N), \quad (4)$$

with

$$\varepsilon=\left|\frac{T-T_N}{T_N}\right|.$$

Thus, the sign of $d\rho/dT$ at T_N is determined by the magnitudes of the coefficients A and B. In the case of the pseudogap-type antiferromagnets, the number of the conduction electrons changes with the onset of the antiferromagnetic ordering, and the first term in Eq. (4) becomes dominant. As a result, $d\rho/dT$ exhibits a minimum at T_N and the $\rho-T$ curve is accompanied by a hump just below T_N. The arrows in Figs. 1(a) and 1(b) indicate T_N defined from the minimum point in the $d\rho/dT-T$ curves. The value of T_N is highest in the vicinity of the equiatomic composition and it gradually decreases with deviating from the equiatomic composition, that is, the highestvalue of T_N observed in the present study is 1145 K for the alloy with 50.1% Ir. The hump just below T_N is not so clear as that of other pseudogap-type antiferromagnetic MnPd (Ref. 10) and MnPt (Ref. 12) alloys. This behavior is very consistent with the band calculations as described in connection with Fig. 6(a).

Concentration dependences of the room temperature lattice constants a, c, and the ratio of c/a of the $L1_0$-type MnIr alloy system are plotted in Fig. 3, together with the previous data.[26] The lattice constants of a and c are 3.855 and 3.644 Å, respectively, thus the c/a ratio is 0.945 for the equiatomic

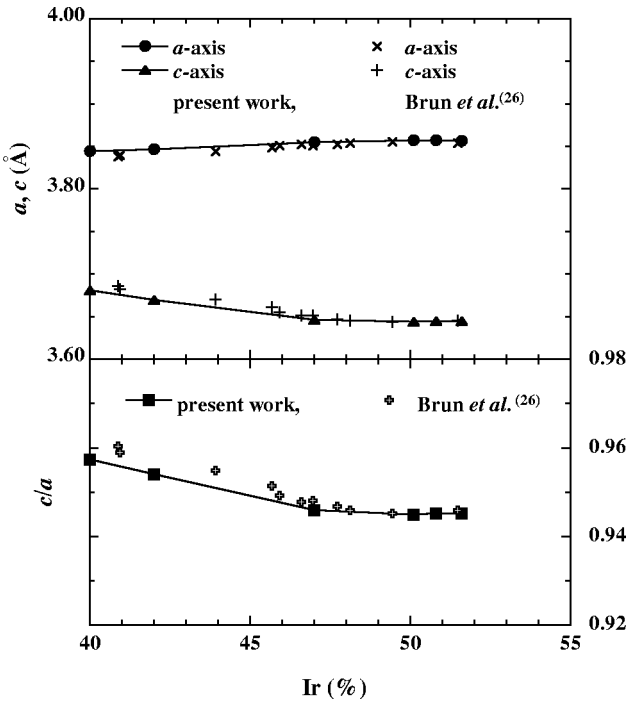

FIG. 3. Concentration dependences of the room temperature lattice constants a, c, and the ratio of c/a of the $L1_0$-type MnIr alloy system, together with the previous data. (Ref. 26).

composition of MnIr. The value of c is comparable to that of the $L1_0$-type equiatomic MnPt alloy, whereas the value of a of MnIr is smaller than that of MnPt,[32] being close to the cubic lattice. In this connection, the room temperature lattice constants of a and c for the $L1_0$-type equiatomic MnPt alloy are 4.002 and 3.672 Å, respectively, and the c/a ratio is 0.918.[32]

Given in Fig. 4 is the concentration dependence of the Néel temperature T_N obtained from the present electrical

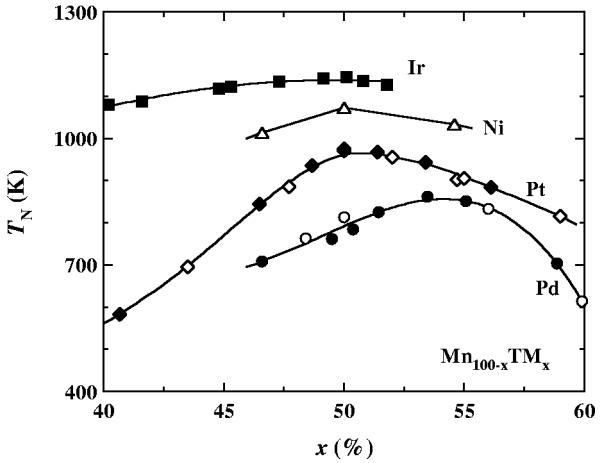

FIG. 4. Concentration dependence of the Néel temperature T_N for the $L1_0$-type MnIr alloy system obtained from the present electrical resistivity measurements, together with that of the $L1_0$-type $Mn_{100-x}TM_x$ [TM=Ni (Ref. 5), Pd (Refs. 5, 32), and Pt (Refs. 5, 12)] alloy systems. The solid and open symbols indicate T_N obtained from our electrical resistivity measurements (Refs. 12, 32) and previous neutron diffractions (Ref. 5), respectively.

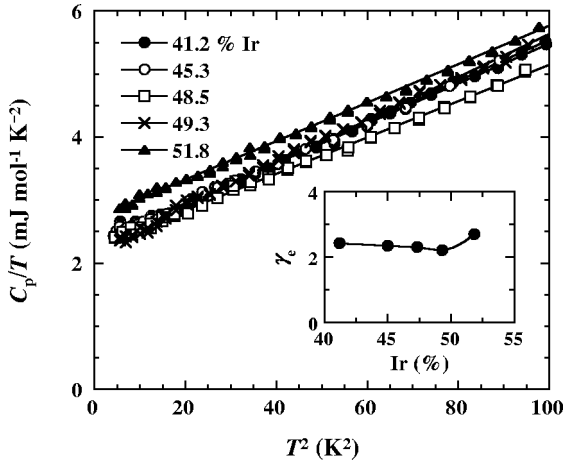

FIG. 5. Low-temperature specific heat capacity C_p in the form of $C_p/T-T^2$ for the $L1_0$-type MnIr alloys. The inset shows the concentration dependence of the electronic specific heat coefficient γ_e in mJ mol^{-1} K^{-2}.

resistivity-temperature, $\rho-T$, curves for the $L1_0$-type MnIr alloy system, together with that for the $L1_0$-type MnNi,[5] MnPd,[5,32] and MnPt (Refs. 5, 12) alloy systems. The solid and open symbols indicate T_N obtained from our electrical resistivity measurements[12,32] and previous neutron diffractions,[5] respectively. From the figure, it is clear that the MnIr alloy system has the highest T_N among these $L1_0$-type Mn alloy systems. In addition, the concentration dependence of T_N for the $L1_0$-type MnIr alloy system is rather insensitive to the Ir concentration, compared with the other $L1_0$-type systems.

The low-temperature specific heat capacity C_p for several kinds of the $L1_0$-type MnIr alloys is shown in the form of $C_p/T-T^2$ in Fig. 5. As shown in the figure, the data are well fitted by a straight line in such low temperature regions. The intercepting point of the ordinate obtained from the linear extrapolation corresponds to the electronic specific heat coefficient γ_e. By neglecting the electron phonon coupling term, the value of γ_e is expressed by

$$\gamma_e = \tfrac{1}{3}\,\pi^2 k_B^2 N(E_F), \tag{5}$$

where k_B and $N(E_F)$ are the Boltzmann constant and the total density of states (DOS) at the Fermi level E_F, respectively. The inset shows the concentration dependence of γ_e in mJ mol^{-1} K^{-2}. The values of γ_e for the MnIr alloys are almost the same value of 2–3 mJ mol^{-1} K^{-2} in the present concentration region. Namely, the magnitude of γ_e is insensitive to the concentration in the same manner as the concentration dependence of T_N. The value of γ_e is much smaller than that of other ordinary transition metals and alloys, indicating a low DOS at E_F, though the value is larger than that of the $L1_0$-type equiatomic MnTM (TM=Ni, Pd, and Pt) alloys.[10,12] Both the experimental and the calculated values of γ_e are listed in Table I for the following discussion.

Figures 6(a) and 6(b) display the calculated local density of states (DOS) of Mn and Ir for the $L1_0$-type equiatomic MnIr alloy in the collinear antiferromagnetic (AF) and in the paramagnetic (PM) states, respectively. The upper and lower

TABLE I. The experimental electronic specific heat coefficient (γ_e in mJ mol^{-1} K^{-2}), the calculated electronic specific heat coefficient ($\gamma_e^{\rm cal}$ in mJ mol^{-1} K^{-2}) obtained by the total density of states (DOS), the experimental Néel temperature (T_N in K), and the calculated Néel temperature ($T_N^{\rm cal}$ in K) given by the effective exchange constant J_0 for the $L1_0$-type equiatomic MnTM [TM=Ir, Ni (Ref. 33), Pd (Refs. 10, 33), and Pt (Refs. 12, 33)]. alloy systems.

	γ_e	$\gamma_e^{\rm cal}$	T_N	$T_N^{\rm cal}$	Reference
MnIr	2.1	~1.0	1145	1495	
MnNi	0.7	~0.3	~1070	1224	5, 33
MnPd	0.3	~0.3	810	1077	5, 10, 33
MnPt	0.2	~0.3	970	953	5, 8, 12, 33

curves refer to the majority and minority spin states, respectively, for the Mn and Ir sites. In the calculations, the lattice constants are settled as $a=3.855$ and $c=3.644$ Å ($c/a=0.945$) deduced from the room temperature x-ray diffraction in Fig. 3. The paramagnetic state can be calculated by the coherent potential approximation (CPA) applying the tight-binding linear muffin-tin orbital (LMTO) method for the system where both the Mn moments pointing upward and downward are distributed randomly in the Mn sublattice. It is evident from the figures that a distinct dip is formed around the Fermi level E_F in the AF state and the DOS curve becomes lower than that in the PM state. The total DOS in the AF state of the equiatomic MnIr alloy is about 6 states Ry^{-1} atom^{-1} spin^{-1} from the figure, corresponding to the electronic specific heat coefficient γ_e of about 1 mJ mol^{-1} K^{-2} using Eq. (5). The experimental electronic specific heat coefficient (γ_e in mJ mol^{-1} K^{-2}), the calculated electronic specific heat coefficient ($\gamma_e^{\rm cal}$ in mJ mol^{-1} K^{-2}) obtained by the DOS are listed in Table I, together with the experimental T_N (T_N in K) and the calculated T_N ($T_N^{\rm cal}$ in K) given by the effective exchange constant J_0 for the $L1_0$-type equiatomic MnTM [TM=Ir, Ni (Refs. 5, 33), Pd (Ref. 10), and Pt (Refs. 12, 33)] alloy systems. Although γ_e of the MnIr alloy is twice as large as $\gamma_e^{\rm cal}$, these values are very small, compared with the data of ordinary transition metals and alloys.

As described above, it is clear that the $L1_0$-type MnIr alloy system is pseudogap-type antiferromagnets from the band calculations, electrical resistivity and low temperature specific heat data. However, γ_e is larger than that of the equiatomic MnPd (Ref. 10) and MnPt (Ref. 12) alloys which exhibit a clear hump in the $\rho-T$ curves and their γ_e is significantly small, about 0.2–0.3 mJ mol^{-1} K^{-2} in the vicinity of the equiatomic composition. That is, the present calculated band structures are in agreement with the experimental results which are not so clear in hump just below T_N in the $\rho-T$ curves and not so significantly small in the value of γ_e, compared with those of equiatomic MnPt and MnPd alloys. The calculated magnetic moments of Mn in the AF and PM states are 2.74 and 2.18 μ_B, respectively. The value of the former is not so different from the experimental value of about 3.4 μ_B at room temperature for $Mn_{51}Ir_{49}$ alloy.[25] Figures 7(a) and 7(b) show the calculated local density of states

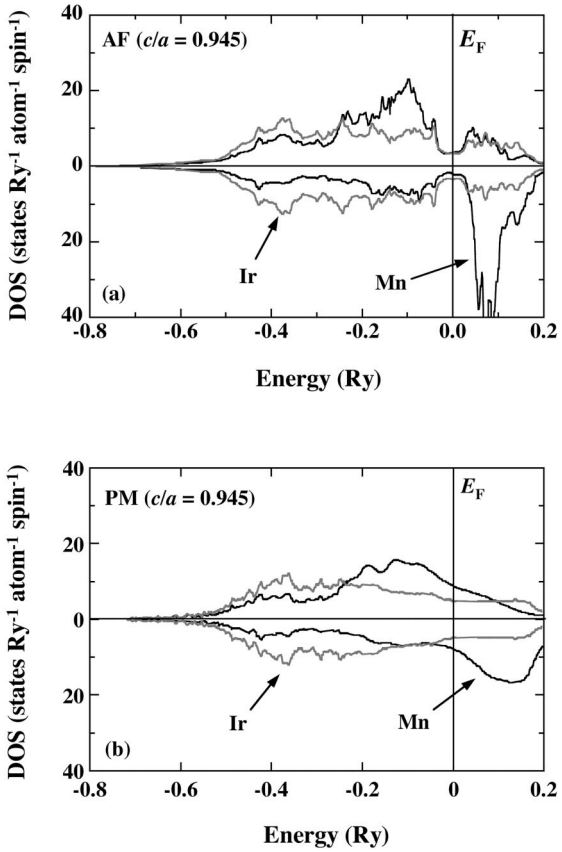

FIG. 6. Density of states of Mn and Ir for the $L1_0$-type equiatomic MnIr alloy calculated by the tight-binding linear muffin-tin orbital (LMTO) method using the experimental lattice constants of the equiatomic MnIr ($c/a=0.945$). The upper and lower curves refer to the majority and minority spin states, respectively, for the Mn and Ir sites. In the figure, (a) and (b) are in the antiferromagnetic (AF) and paramagnetic (PM) states, respectively.

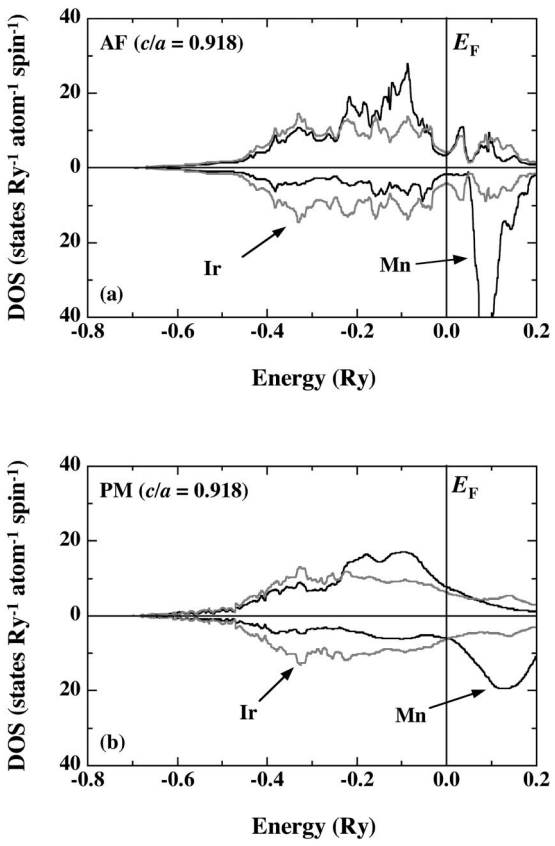

FIG. 7. Density of states of Mn and Ir for the $L1_0$-type equiatomic MnIr alloy calculated by using the lattice constants for the equiatomic MnPt alloy ($c/a=0.918$) (Ref. 32). In the figure, (a) and (b) are in the antiferromagnetic (AF) and paramagnetic (PM) states, respectively.

(DOS) of Mn and Ir for the $L1_0$-type equiatomic MnIr in the collinear antiferromagnetic (AF) and in the paramagnetic (PM) states, respectively, replacing the lattice constants of the $L1_0$-type equiatomic MnPt alloy, settled as $a=4.002$ and $c=3.672$ Å ($c/a=0.918$) by using our experimental results.[32] Comparing with Fig. 6(a), the total DOS at E_F is larger and the whole of the bandwidth is slightly narrower, reflecting the increase of the lattice constants. The calculated magnetic moments of Mn in the AF state and the PM states are 3.12 and 2.86 μ_B, respectively.

Shown in Fig. 8 is the effective exchange constant J_0 of the $L1_0$-type equiatomic MnIr alloy as a function of the Fermi level E_F calculated by using the experimental lattice constants of MnIr ($c/a=0.945$) (a) and the J_0 curve obtained by using the lattice constant of the $L1_0$-type equiatomic MnPt alloy ($c/a=0.918$) (b) instead of the lattice constants of the $L1_0$-type equiatomic MnIr, together with the J_0 curve for the $L1_0$-type equiatomic MnPt alloy itself using the lattice constants ($c/a=0.918$) (c).[32,33] The actual Fermi level E_F is located at the origin of the abscissa and the value of J_0 at $E_F=0$ is 193 meV in (a). The calculated Néel temperature T_N^{cal} from Eq. (3) is 1495 K in permissible value by considering the fact that the higher value of T_N by 20%–30% would be adequate within the molecular field approximation for three-dimensional system. As listed in Table I, the values of T_N^{cal} of the $L1_0$-type equiatomic MnNi,[33] MnPd,[10] and MnPt (Ref. 12) alloys obtained from J_0 in the same manner are 1224, 1077, and 953 K, respectively. Therefore, T_N^{cal} of MnIr is also highest among these systems. The calculated magnetic moments of Mn ($m_{\mathrm{Mn}}^{\mathrm{cal}}$ in μ_B) in the AF and PM states, the effective exchange constant (J_0 in meV) and the calculated Néel temperature (T_N^{cal} in K) obtained from the curves (a), (b), and (c) are also listed in Table II. The feature of J_0 curves (a) and (b) is very similar to each other, although the magnitude of J_0 at $E_F=0$ is slightly different. The difference between J_0 of two curves is 14 meV, corresponding to be about 100 K in T_N. Moreover, by comparing the J_0 curve of the MnIr (a) with that of the MnPt (c), the former shifts to a higher energy side, as a result, the position of $E_F=0$ comes close to the maximum of the peak in the J_0 curve. This causes a large difference in J_0 of 70 meV between two curves (a) and (c), corresponding to be about 540 K in T_N. It is evident that the difference between the number of electrons of Ir and Pt gives a larger contribution to J_0 rather than the difference between the lattice constants and/or the c/a ratio. Consequently, the magnitude of T_N for the $L1_0$-type equiatomic Mn alloy system is dominantly gov-

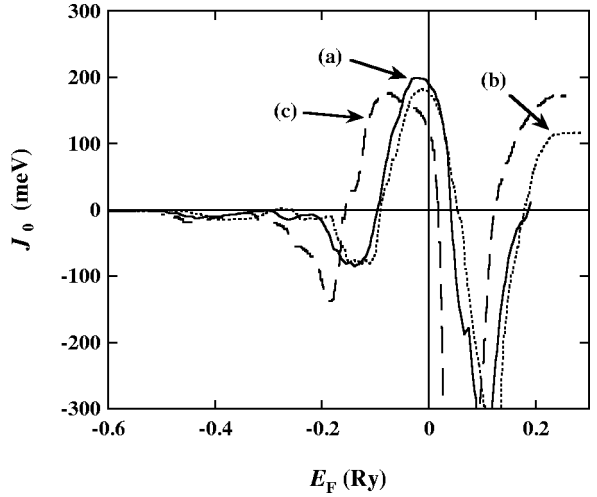

FIG. 8. The effective exchange constant J_0 as a function of the Fermi level E_F. (a) $L1_0$-type equiatomic MnIr alloy calculated by using the experimental lattice constants ($c/a=0.945$). (b) $L1_0$-type equiatomic MnIr alloy obtained by using the lattice constants of the $L1_0$-type equiatomic MnPt alloy ($c/a=0.918$). (c) $L1_0$-type equiatomic MnPt alloy itself calculated by using the lattice constants ($c/a=0.918$) (Refs. 32, 33).

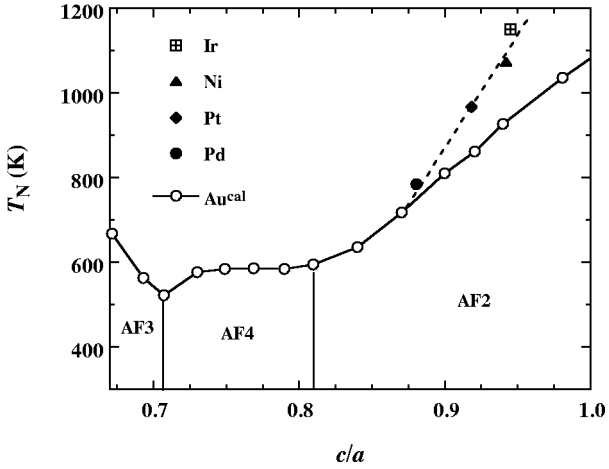

FIG. 9. The calculated Néel temperature T_N^{cal} as a function of the c/a ratio for the $L1_0$-type equiatomic MnAu alloy (Refs. 36, 37) together with the experimental T_N of the $L1_0$-type equiatomic MnTM [TM=Ni (Ref. 5), Pd (Ref. 10), Pt (Ref. 12), and Ir] alloys.

erned by the number of the electrons at the Mn site in analogy with the γ-Mn system alloys.[34,35]

Next, we show the Néel temperature T_N^{cal} calculated by the Monte Calro simulations based on the Hisenberg model as a function of the c/a ratio in Fig. 9 for the $L1_0$-type equiatomic MnAu alloy,[36,37] together with the experimental values of T_N for the $L1_0$-type equiatomic MnTM (TM=Ni,[5] Pd,[10] Pt,[12] and Ir) alloys. In the figure, AF2, AF3, and AF4 phases stand for the collinear-type antiferromagnetic spin configurations determined by calculating the total energies. The detailed spin configurations in each phase are in the references.[36,37] Since the equiatomic MnAu has a crystal structure slightly deformed from the $B2$ (CsCl)-type structure, the calculations were performed as a function of the c/a ratio in the $L1_0$-type structure with the fixed volume of the experimental data.[38] The calculated magnetic structure and T_N^{cal} for the equiatomic MnAu in which the c/a ratio corresponds to 0.7 in the $L1_0$-type are in accord with the experimental one.[38] It is worth noting that T_N^{cal} linearly increases with the value of the c/a ratio in the AF2 phase region, in which the c/a ratio varies from 0.85 to 1.00. The relation between the values of T_N^{cal} for the $L1_0$-type equiatomic MnAu alloy and the c/a ratio is qualitatively in agreement with the experimental data. Strictly speaking, the experimental results of T_N for the $L1_0$-type equiatomic MnTM alloys deviate from the theoretical line for the MnAu alloy as given by the dashed line in the figure. This would be caused by the fact that the spin configuration of MnTM is not AF2 but AF1, and the number of electrons is different between Au and TM elements. Consequently, the data given in Fig. 9 tell us that the lattice constant and/or the c/a ratio also contribute to the magnitude of T_N to a certain extent, although the number of electrons at the Mn site dominates T_N in the $L1_0$-type equiatomic Mn alloy systems as discussed in connection with Figs. 8(a) and 8(c).

TABLE II. The calculated magnetic moments of Mn (m_{Mn}^{cal} in μ_B) in the antiferromagnetic AF and paramagnetic PM states, the effective exchange constant (J_0 in meV) and the calculated Néel temperature (T_N^{cal} in K) of the $L1_0$-type equiatomic MnIr and MnPt (Refs. 12, 33) alloys. (a) The values calculated by using the experimental lattice constants of MnIr, (b) the values of MnIr alloy, using the lattice constants of MnPt instead of those of MnIr, and (c) the values of MnPt, using the lattice constants of MnPt.

	m_{Mn}^{cal} (AF)	m_{Mn}^{cal} (PM)	J_0	T_N^{cal}
MnIr (a)	2.74	2.18	193	1495
MnIr (b)	3.12	2.86	179	1387
MnPt (c)	3.22	2.99	123	953

Finally, we discuss the present results from practical viewpoints. For applications to GMR and TMR devices, it is desired that the antiferromagnetic materials for the pinning layer has a high Néel temperature T_N in order to obtain the excellent properties, because it is well known that the higher T_N the antiferromagnetic layer, the higher blocking temperature the exchange bias film.[39,40] Although the $L1_0$-type equiatomic MnPt alloy is considered to be most advantageous, it has been pointed out that useful concentration region is very narrow and restricted in the vicinity of the equiatomic composition.[41] This is understood from the fact that T_N of the MnPt alloy system is sensitive to the Pt concentration as shown in Fig. 4. On the other hand, T_N of the MnIr alloy system is not only very high but also insensitive to the Ir concentration, therefore, the MnIr alloy system would be more useful for application. In the case of multilayer spin valves, thermal treatments such as annealing are necessary to obtain the $L1_0$-type structure. For example, the MnPt alloy system needs annealing around at 550 K for several hours.[13–18] In the equilibrium state, the transformation temperature from the $L1_0$-type structure to the $B2$-type structure in the MnIr alloy system is lower than that of the MnPt alloy system by about 110 K.[4] Accordingly, we can expect a lower

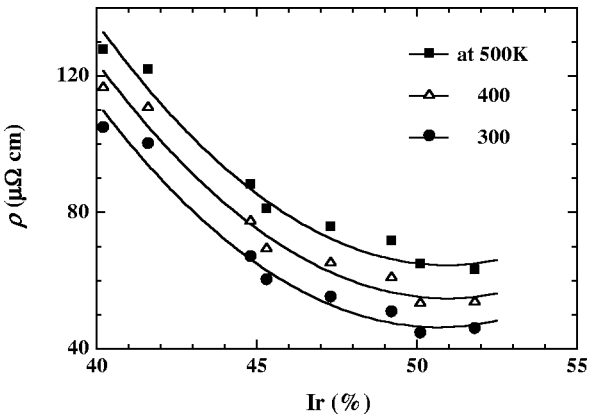

FIG. 10. Concentration dependence of electrical resistivity ρ at 300, 400, and 500 K for the $L1_0$-type MnIr alloy system.

annealing temperature in spin valves for the MnIr film, compared with that for the MnPt film. In addition, the electrical resistivity is also very important factor to select the antiferromagnetic materials because recent interest is how to design the spin-valves by using films with low resistivity.[18] For example, the so-called current perpendicular to plane (CPP)-type spin-valves are suitable for the narrow gap spacing in the recording media,[42,43] and hence the resistivity of the antiferromagnetic layer should be diminished because the antiferromagnetic layer is relatively thick in the spin-valve multilayers. The reduction of electrical resistivity of the antiferromagnets would bring about further progresses of magnetoresistance (MR) devices. From practical viewpoints, the concentration dependence of electrical resistivity ρ at 300, 400, and 500 K is given in Fig. 10 for the $L1_0$-type MnIr alloy system. It is clear from the figure that the value of ρ is lowest in the vicinity of the equiatomic composition and the concentration dependence of ρ is not so sensitive to the Ir concentration, in analogy with the concentration dependence of T_N, compared with those in the MnPt alloy system.[32] Because the antiferromagnetic layer is thick, compared to other magnetic layer in the GMR and TMR devices, it is necessary to select carefully the alloy system and the concentration in the antiferromagnetic alloys. It is concluded that the $L1_0$-type MnIr alloy system is expected to be one of the promising alloy systems for the pining layer of the exchange bias-field films, because the magnetic and electrical properties required for spin-valve are less sensitive to the Ir concentration, compared with those of other $L1_0$-type Mn alloy systems.[12,32] Investigations of spin-valve characteristics for the $L1_0$-type MnIr alloy system are highly desired in order to develop high performance devices.

IV. CONCLUSION

To discuss the Néel temperature T_N and the electronic state of the $L1_0$-type MnIr alloy system, the measurements of electrical resistivity and low temperature specific heat capacity have been carried out. Furthermore, the band calculations have been performed by using the tight-binding linear muffin-tin orbital (LMTO) method with the local spin density (LSD) functional theory, and the value of T_N was estimated from the effective exchange constant J_0 obtained from the molecular field approximation. The experimental results pesent the characteristic behaviors of pseudogap-type antiferromagnets, and the values of T_N and the electronic specific heat coefficient γ_e correlated to the density of states at the Fermi level E_F are in harmony with the theoretical results. Practically, the less sensitive magnetic and electrical properties against the Ir concentration are expected to be useful. The main results are summarized as follows:

(1) The electronic specific heat coefficient γ_e in the concentration region from 40% to 52% Ir is $2-3\,\mathrm{mJ\,mol^{-1}\,K^{-2}}$, indicating very low density of states. The band calculations also reveal a distinct dip around the Fermi level E_F in the antiferromagnetic state, consistent with the experimental results.

(2) The temperature dependence of electrical resistivity exhibits a hump just below T_N, characteristic to pseudogap-type antiferromagnets. The magnetic and electrical properties are not so sensitive to the Ir concentration, compared with those of other $L1_0$-type Mn alloy systems.

(3) The theoretical and experimental values of the Néel temperature T_N of the $L1_0$-type equiatomic MnIr alloy are highest among several kinds of the $L1_0$-type equiatomic Mn alloys.

(4) For the high value of T_N of the $L1_0$-type Mn alloy systems, the control of the number of electrons at the Mn site is important as well as the formation of the pseudogap in the density of states.

ACKNOWLEDGMENTS

The authors wish to express thanks to Mr. Y. Okamoto for his experimental support in the present study. Two of the authors (R.Y. Umetsu and M. Miyakawa) have been supported by the Research Foundation of the Japan Society for the Promotion of Science for Young Scientists. The present study has been made under the support of a Grant-in-Aid for Scientific Research (B)(2), No. 13450225, from the Japan Society for the Promotion of Science.

[1] B. R. Coles and W. Hume-Rothery, J. Inst. Met. **80**, 85 (1951).
[2] J. S. Kasper and J. S. Kouvel, J. Phys. Chem. Solids **11**, 231 (1959).
[3] E. Raub and W. Mahler, Z. Metallkd. **45**, 430 (1954).
[4] E. Raub and W. Mahler, Z. Metallkd. **46**, 282 (1955).
[5] L. Pál, E. Krén, G. Kádár, P. Szabó, and T. Tarnóczi, J. Appl. Phys. **39**, 538 (1968).
[6] A. Kjekshus, R. Møllerud, A. F. Andresen, and W. B. Pearson, Philos. Mag. **16**, 1063 (1967).
[7] A. F. Andresen, A. Kjekshus, R. Møllerud, and W. B. Pearson, Philos. Mag. **11**, 1245 (1965).
[8] E. Krén, G. Kádár, L. Pál, J. Sólyom, P. Szabó, and T. Tarnóczi,

Phys. Rev. **171**, 574 (1968).
[9] A. Sakuma, J. Magn. Magn. Mater. **187**, 105 (1998).
[10] R. Y. Umetsu, K. Fukamichi, and A. Sakuma, J. Magn. Magn. Mater. **239**, 530 (2002).
[11] A. Sakuma, J. Phys. Soc. Jpn. **69**, 3072 (2000).
[12] R. Y. Umetsu, K. Fukamichi, and A. Sakuma, J. Appl. Phys. **91**, 8873 (2002).
[13] S. Prakash, K. Pentek, and Y. Zhang, IEEE Trans. Magn. **37**, 1123 (2001).
[14] M. Saito, N. Hasegawa, F. Koike, H. Seki, and T. Kuriyama, J. Appl. Phys. **85**, 4928 (1999).
[15] A. Khapikov, B. Simion, and M. Lederman, J. Appl. Phys. **93**, 7313 (2003).
[16] E. H. Morales, Y. Wang, D. Lederman, A. J. Kellock, and M. J. Carey, J. Appl. Phys. **93**, 4729 (2003).
[17] M. M. Schwickert, J. R. Childress, R. E. Fontana, A. J. Kellock, P. M. Rice, M. K. Ho, T. J. Thompson, and B. A. Gurney, J. Appl. Phys. **89**, 6871 (2001).
[18] J. R. Childress, M. M. Schwickert, R. E. Fontana, M. K. Ho, P. M. Rice, and B. A. Gurney, J. Appl. Phys. **89**, 7353 (2001).
[19] S. Araki, K. Sato, T. Kagami, S. Saruki, T. Uesugi, N. Kasahara, T. Kuwashima, N. Ohta, J. Sun, K. Nagai, S. Li, N. Hachisuka, H. Hatate, T. Kagotani, N. Takahashi, K. Ueda, and M. Matsuzaki, IEEE Trans. Magn. **38**, 72 (2002).
[20] K. Hoshino, R. Nakatani, H. Hoshiya, Y. Sugita, and S. Tsunashima, Jpn. J. Appl. Phys., Part 1 **35**, 607 (1996).
[21] H. N. Fuke, K. Saito, Y. Kamiguchi, H. Iwasaki, and M. Sahashi, J. Appl. Phys. **81**, 4004 (1997).
[22] A. J. Devasahayam, P. J. Sides, and M. H. Kryder, J. Appl. Phys. **83**, 7216 (1998).
[23] D. Wang, M. Tondra, C. Nordman, and J. M. Daughton, IEEE Trans. Magn. **35**, 2886 (1999).
[24] S. Tehrani, J. M. Slaughter, E. Chen, M. Durlam, J. Shi, and M. DeHerrera, IEEE Trans. Magn. **35**, 2814 (1999).
[25] K. Selte, A. Kjekshus, A. F. Andresen, and W. B. Pearson, Acta Chem. Scand. (1947-1973) **22**, 3039 (1968).
[26] K. Brun, A. Kjekshus, and W. B. Pearson, Acta Chem. Scand. (1947-1973) **19**, 107 (1965).
[27] A. I. Liechtenstein, M. I. Katsnelson, and V. A. Gubanov, Solid State Commun. **54**, 327 (1985).
[28] A. Sakuma, J. Phys. Soc. Jpn. **68**, 620 (1998).
[29] J. Kudrnovský and V. Drchal, Phys. Rev. B **41**, 7515 (1990).
[30] P. L. Rossiter, *The Electrical Resistivity of Metals and Alloys* (Cambridge University Press, Cambridge, 1987).
[31] Y. Suezaki and H. Mori, Prog. Theor. Phys. **41**, 1177 (1969).
[32] R. Y. Umetsu, K. Fukamichi, and A. Sakuma (unpublished).
[33] A. Sakuma and K. Fukamichi, in *Advanced Magnetic Materials*, edited by Y. Liu, D. J. Sellmyer, and D. Shindo (Springer, in press).
[34] R. Yamauchi, K. Fukamichi, H. Yamauchi, and A. Sakuma, J. Alloys Compd. **279**, 93 (1998).
[35] R. Yamauchi, K. Fukamichi, H. Yamauchi, A. Sakuma, and J. Echigoya, J. Appl. Phys. **85**, 4741 (1999).
[36] J.-T. Wang, D.-S. Wang, and Y. Kawazoe, Appl. Phys. Lett. **79**, 1507 (2001).
[37] J.-T. Wang, D.-S. Wang, and Y. Kawazoe, Mater. Trans. **44**, 1529 (2003).
[38] G. E. Bacon and R. Street, Proc. Phys. Soc. (London) **72**, 470 (1958).
[39] R. F. C. Farrow, R. F. Marks, S. Gider, A. C. Marley, S. S. P. Parkin, and D. Mauri, J. Appl. Phys. **81**, 4986 (1997).
[40] A. Veloso, P. P. Freitas, N. J. Oliveira, J. Fernandes, and M. Ferreira, IEEE Trans. Magn. **34**, 2343 (1998).
[41] K. M. Krishnan, C. Nelson, C. J. Echer, R. F. C. Farrow, R. F. Marks, and A. J. Kellock, J. Appl. Phys. **83**, 6810 (1998).
[42] M. A. M. Gijs, S. K. J. Lenczowski, and J. B. Giesbers, Phys. Rev. Lett. **70**, 3343 (1993).
[43] M. Takagishi, K. Koi, M. Yoshikawa, T. Funayama, H. Iwasaki, and M. Sahashi, IEEE Trans. Magn. **38**, 2277 (2002).